Vacuum 231 (2025) 113757

Contents lists available at ScienceDirect

Vacuum

journal homepage: www.elsevier.com/locate/vacuum

Effect of hydrogen ion irradiation on the mechanical properties of thermally aged Z3CN20.09M duplex stainless steel

Penghui Lei [a], Ni Jiang [b,c], Jiannan Hao [d], Qing Peng [d,**], Pan Qi [e], Fangjie Shi [f], Yuhua Hang [f], Qianwu Li [f], Chao Ye [b,c,*]

[a] School of Nuclear Science and Technology, Xi'an Jiaotong University, Xi'an, 710049, China
[b] Institute of Clean Energy, Yangtze River Delta Research Institute, Northwestern Polytechnical University, Taicang, 215400, China
[c] School of Materials Science and Engineering, Northwestern Polytechnical University, Xi'an, 710072, China
[d] State Key Laboratory of Nonlinear Mechanics, Institute of Mechanics, Chinese Academy of Sciences, Beijing, 100190, China
[e] China Nuclear Power Operation Technology Corporation, LTD, Wuhan, 430223, China
[f] Suzhou Nuclear Power Research Institute, Suzhou, 215004, China

ARTICLE INFO

Handling Editor: Prof. L.G. Hultman

Keywords:
Z3CN20.09M duplex alloy
Hydrogen ions irradiation
Nanohardness
TEM in-situ tensile test

ABSTRACT

In order to investigate the synergistic effect of thermal aging and hydrogen, Z3CN20.09M duplex stainless steels (DSS) were thermal aged at 400 °C and then the irradiated by hydrogen ions. Due to the segregation of the Fe and Cr elements induced by spinodal decomposition, the nanohardness of the ferrite phase increased after thermal aging process. The irradiation effects by hydrogen ion could further increase the nanohardness of the damage region. But the {011}<111> slip system structures formed by the irradiation significantly suppressed the hardening effects of the ions irradiation induced dislocations and spinodal decomposition induced element segregation. During the in-situ transmission electron microscopy (TEM) tensile process, severe deformation occurred and extended along a slip band that ran diagonally across the entire sample region. At last, a cracking formed at the deformation center area and propagated along the crack tip towards the irradiation damage side, ultimately leading to the sample fracture. This study serves as a valuable reference for improving the properties of Z3CN20.09M DSS utilized in nuclear plants.

1. Introduction

Z3CN20.09M DSS are widely used as the main pipeline material of the primary circuit system in reactors and have been safely served in Daya Bay nuclear plants in China for about 30 years [1,2]. During the prolonged high-temperature service, the spinodal decomposition induced thermal aging embrittlement (TAE) tend to occur in the Z3CN20.09M DSS, which is due to segregation of Cr and Fe elements in ferrite with the nanoscale (Cr-rich α′ phases distribute in the Fe-rich α matrix phases) [3,4]. Essentially, the internal coherency strain formed by the lattice mismatch between α' and α phases lead to TAE [5,6], which is always the key concern for the practical application of DSS in reactors. The deterioration of mechanical properties caused by structural and compositional changes in ferrite will seriously affect the safe operation of the reactors in the later stage of its service life. The changes of the microstructure and compositions in ferrite after thermal aging have been extensively studied [7–9].

On the other hand, the inner side of the main pipeline is in contact with the cooling water in the first loop, which contains a large amount of hydrogen mainly from the reaction between the Zr alloy cladding tube and cooling water [10,11], the transmutation gas H_2 produced by the nuclear fuel reaction [12], the radiation induced water splitting [13] and the H ions of the chemicals (H_3BO_3) in the cooling water [14,15]. In addition to the explosion accident of Fukushima nuclear power plant that caused by the accumulation of hydrogen gas [16–18], hydrogen can also result in the mechanical properties degradation of reactor structural component materials, including Zr cladding material [19–21], pressure vessel steel [22,23] and primary circuit main pipeline [24]. The hydrogen embrittlement for Zr alloy cladding has been researched a lot in recent decades [25,26]. While the effect of hydrogen on the dual phase steel material used in the main pipeline is relatively little. During the electrochemical hydrogen charging process, micro stretching and

* Corresponding author. Institute of Clean Energy, Yangtze River Delta Research Institute, Northwestern Polytechnical University, Taicang, 215400, China.
** Corresponding author. State Key Laboratory of Nonlinear Mechanics, Institute of Mechanics, Chinese Academy of Sciences, Beijing, 100190, China.
E-mail addresses: PengQing@imech.ac.cn (Q. Peng), yechao@nwpu.edu.cn (C. Ye).

https://doi.org/10.1016/j.vacuum.2024.113757
Received 20 September 2024; Received in revised form 17 October 2024; Accepted 19 October 2024
Available online 20 October 2024

calculation results indicate that the hydrogen atoms are trapped at the phase boundary, increasing the hardness of the ferrite phase but reducing the hardness of the austenite phase, while once the boundary is passivated, further hydrogen entering can rapidly diffuse without energy barriers, leading to two-phase softening [27]. Besides, X-ray micro-diffraction analysis results reveal that the electrochemical hydrogen absorption in duplex steels can lead to swelling of austenite lattice, but the lattice parameter of the ferrite phase remains unchanged during this process [28]. The synergistic effect of thermal aging and hydrogen on the microstructure evolution and properties of the Z3CN20.09M DSS materials has not been fully understood.

Based on the actual service conditions of the main pipeline in the reactors, in this work, the internal microstructure evolutions of the Z3CN20.09M DSS materials under the synergistic effect of thermal aging and hydrogen were investigated by using hydrogen ion implantation after thermal aging process.

2. Experimental methods

Z3CN20.09M duplex stainless steels made in France are being researched for thermal aging and ions irradiation induced microstructure evolution and mechanical property degradation. The chemical composition of Z3CN20.09M DSS is as follows (in wt.%): Cr-20.893, Mo-0.103, Si-1.020, Ni-9.760, Mn-1.058, N-0.045, C-0.026, and Fe-Balance. The surface morphology and phase composition of materials are presented in Fig. 1(a) and (b). During the accelerated thermal aging process, two large steel bulks were aged in two large muffle furnaces at 400 °C for 0 h–3000 h, respectively, and the chamber temperatures were controlled by UDIAN programmable controllers at an accuracy of $<\pm1$ °C using K-type thermocouples; the spatial temperature variation within chamber was ±5 °C. After thermal aging, parts of samples were performed by ions irradiation, 200 keV H^+ ions with a fluence of 6×10^{16} ions/cm^2 were pre-implanted at room temperature using the NEC 400 kV ion implanter under a vacuum of 5×10^{-7}Pa at Xiamen University [29]. Ion irradiation was conducted under high vacuum conditions to prevent residual gas contamination of the vacuum chamber and to avoid oxidation of the sample during the irradiation process. The direction of the ion incidence is perpendicular to the surface of the sample. Based on full damage cascades mode, the displacement threshold energies of main component elements Fe, Cr and Ni were set as 40 eV in the Stopping and Range of Ions in Matter (SRIM) simulation software during the calculation of irradiation parameters [30]. The density of the Z3CN20.09M DSS samples was set as 7.8 g/cm^3 in the SRIM calculations, which was measured by Archimedes' drainage method. Fig. 1(c) displays the simulation results of the depth variation of damage and the concentration of H atoms, which show that the peak displacement damage (approximately 0.65 dpa, displacement per atom), peak hydrogen concentration (approximately 4 %), located at a depth of approximately 880 nm and 950 nm, respectively.

The surface morphologies and microstructures of those unirradiated, irradiated, and annealing samples were characterized by scanning electron microscopy (SEM, Zeiss Gemini 460) under a vacuum of less than 5×10^{-5}Pa, TEM (FEI talos F200X) under a vacuum of 1.1×10^{-7}Pa, selected area electron diffraction (SAED) patterns, scanning transmission electron microscopy (STEM) with electron diffraction spectroscopy (EDS). The TEM samples, less than 100 nm thick, were prepared by using the focused ion beam (FIB, Thermo Scientific Helios G4) lift-out technique. The initial lift-outs were performed by using 30 kV Ga^+ ions with a current of 9.3 nA. During the process of thinning, the energy and current of Ga^+ ions beam was progressively decreased to minimize damage to the sample surface. Final thinning was performed using 2 kV Ga^+ ion. Fig. 1(b) shows the overview image of FIB-prepared TEM sample, the irradiation direction and damage areas are marked. In addition, a 500h-aged sample was machined to a piece of 2 μm × 2.5 μm rectangle with a thickness of about 100 nm by the focused ion beam (FIB, Thermo Scientific, Helios 5 CX) under a vacuum of 4.9×10^{-5}Pa. Transmission electron microscopy (TEM, FEI talos F200X) equipped with stretching table (Instec) was used to perform the TEM in-situ tensile test. The nano-hardness of samples were measured by Hysitron Ti-980 Tribo Indenter, the indentation depth was 100 nm, which are corresponding to the surface region and peak damage region, respectively. In addition, considering the depth of the irradiation damage zone and the impact on the unirradiated area nanohardness indentation tests were performed for each sample at the depth of 100 nm and the results were averaged over 10 measurements.

3. Results and discussion

The spinodal decomposition processes always occur in the duplex stainless steels under the thermal service environments, resulting in the nanoscale segregation of Cr and Fe elements in ferrite. The STEM images of the Z3CN20.09M DSS samples and EDS mapping results of the Cr element inside the ferrite phase in the samples aged at different times are shown in Fig. 2. It shows that the density of defects in the austenite region (A) is much more than the ferrite region (F) in the samples under the original and aged states. For the EDS mapping results in the ferrite

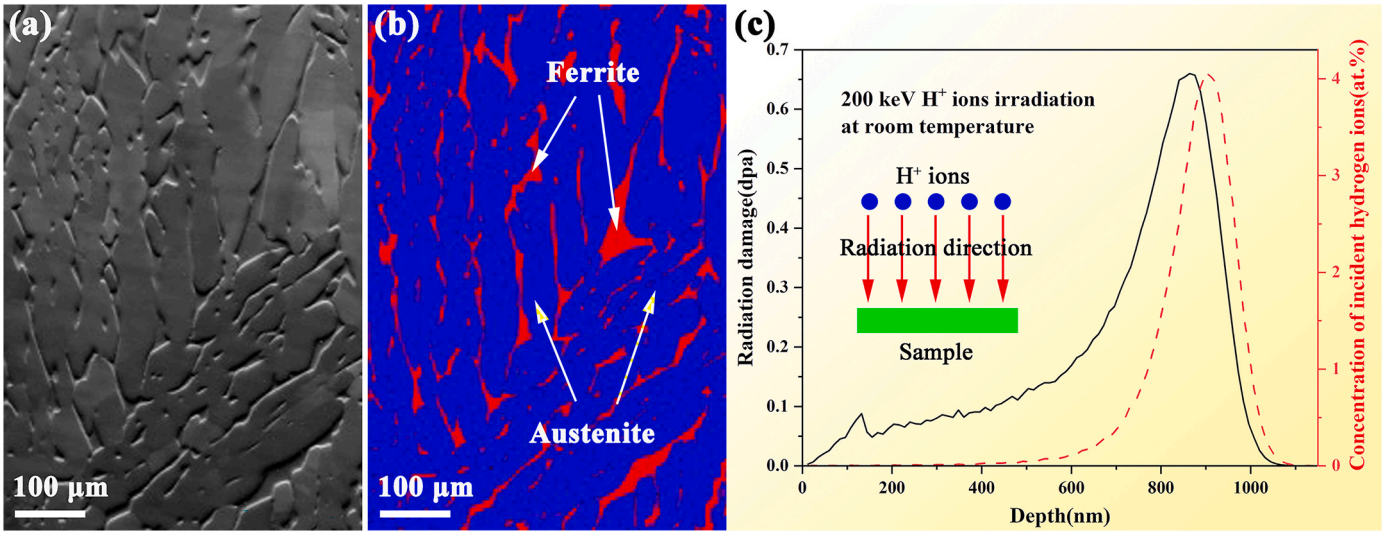

Fig. 1. (a) SEM image for the surface morphology of the as-received Z3CN20.09M DSS sample; (b) The corresponding EBSD phase distribution diagram of (a); (c) the results showing the variation of dpa and hydrogen atom concentrations in the irradiated Z3CN20.09M DSS sample calculated by SRIM 2013 software.

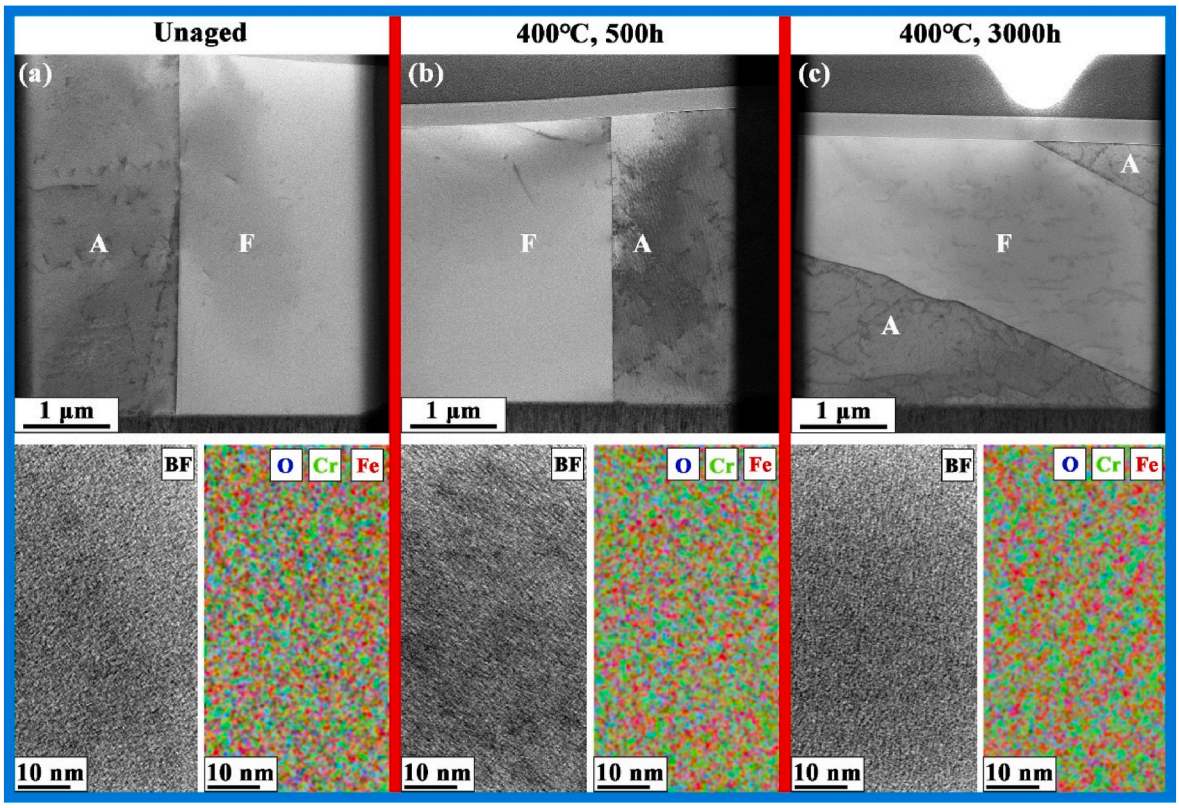

Fig. 2. Overview bright field STEM images of the Z3CN20.09M CDSS samples and the corresponding EDS mapping results in ferrite phase regions of the Z3CN20.09M CDSS samples under different 400 °C thermal aging times: (a) 0 h; (b) 500 h and (c) 3000 h.

region, the green areas represent the aggregation of Cr atoms and the red areas are the Fe atoms. The estimated domain area slightly increases with increasing aging times, from 0.39 nm^2 for 0 h to 1.15 nm^2 for 500 h, and then further increases to 1.83 nm^2 for 3000 h. The presence of a small amount of O element is attributed to the oxidation of the FIB sample surface. There are no significant changes in the distribution of the O element during the thermal aging process. It is clear that the enrichment of Cr and Fe elements occurred with the continue of the thermal aging process, which in line with the previous report by Zhou et al. [31].

The nanohardness results of the ferrite phase under H ions irradiation and thermal aging process are shown in Fig. 3. It is clear that under a single thermal aging effect, the nanohardness of the ferrite phase increases with the increase of thermal aging time, as shown in Fig. 3(a), which is due to the nanoscale periodic fluctuations of the Fe and Cr atomic concentrations induced by spinodal decomposition during the thermal aging process [32,33]. The internal coherency strain induced by the slight lattice mismatch between α′ and α phases can lead to the

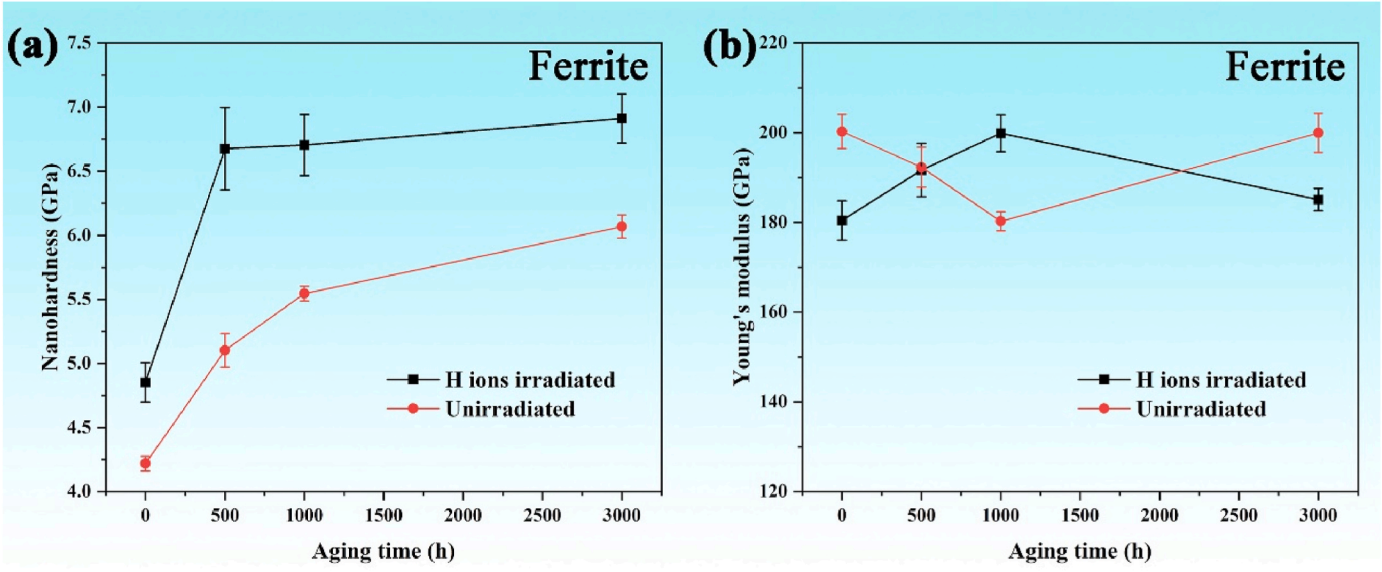

Fig. 3. Nano hardness results of Z3CN20.09M CDSS before and after H ions irradiation under 0–3000 h thermal aging times.

increase of hardness the ferrite [34]. On the other hand, generally, ions irradiation could introduces a large number of defects, resulting in an increase in the hardness of materials [35,36]. Therefore, compared with the unirradiated samples, after the injection of hydrogen ions, the nanohardness of the damage region in the radiated Z3CN20.09M samples significantly increased. However, the increase in hardness of irradiated samples with aging time was not significant during the 500~3000-h thermal aging process, which indicates that the hydrogen ion implantation could weaken the hardening effect induced by spinodal decomposition during thermal aging process. Similar metal softening phenomena were also observed under electrochemical hydrogen charging and atmospheric hydrogen charging conditions [37,38]. Currently, two kinds of theories to explain the mechanism of hydrogen induced metal softening: 1) The suppression of work-hardening [39–42], including the enhancement of cross-slip induced by hydrogen, the decrease of the repulsive interactions between dislocations result from the shielding effect of hydrogen on elastic field; 2) The decrease of shear modulus, dislocation line energy and the increase of dislocation mobility [43,44]. The Young's modulus of irradiated and non-irradiated samples did not show significant changes with aging time, but a turning point appeared at 1000 h, as seen in Fig. 3(b), which might be attributed to the combined effects of element segregation and H ions irradiation. During the 0~1000h thermal aging stage, the material hardening induced by spinodal decomposition and the decrease in elasticity played a dominant role; during the 1000–3000 thermal aging stage, hydrogen induced softening suppressed the previous hardening effect and enhanced the material's plasticity.

Fig. 4 shows the TEM images of Z3CN20.09M CDSS sample that aged at 400 °C for 500 h and then irradiated by H ions at RT temperature. Compared to the austenite phase, the irradiation damage region in the ferrite region can be clearly visible and the boundary between the damaged and undamaged areas is marked in Fig. 4(a). Enlarging a local damage area of the ferrite region, it can be observed that a large number of dislocation line structures were induced by the hydrogen ions irradiation, as shown in Fig. 4(b), which could promote the hardening of materials. By rotating the TEM sample to the vicinity of the nearly [011] crystal band axis, a large number of regularly arranged {011}<111> slip system structures can be observed, as seen in Fig. 4(c). Enlarging the area that marked by red dash frame in Fig. 4(c), the slip layer fault structures are plainly displayed in Fig. 4(d). Therefore, after the implantation of hydrogen ions, a large amount of cross-slip structures formed in the irradiated ferrite area of the samples, which significantly suppressed the hardening effects of the ions irradiation induced dislocations and spinodal decomposition induced element segregation, consistent with hydrogen induced metal softening theory mentioned above [39–42].

In order to further understand the effect of irradiated hydrogen on the microstructure changes of materials during the stretching process, TEM in-situ stretching experiment was conducted, and the initial sample is the ferrite phase of the Z3CN20.09M CDSS aged at 400 °C for 500 h, half of the region is the H-irradiated area, and the other is the unirradiated area, as shown in Fig. 5(a). There are significant differences in the overall microstructure images between these two regions. Under the dark field condition, the severe hydrogen irradiation damage region that near the surface is clearly displayed, which is marked in Fig. 5(e). Fig. 5 (b) shows that when the stroke of the stretching rod increased to 85 nm, a slip band that diagonally spanned the entire region gradually appeared, and the elongation of the hydrogen damage area indicated that the TEM sample also had significant elongation, as seen in Fig. 5(f). When the stretching length reached 593 nm, the microstructure was

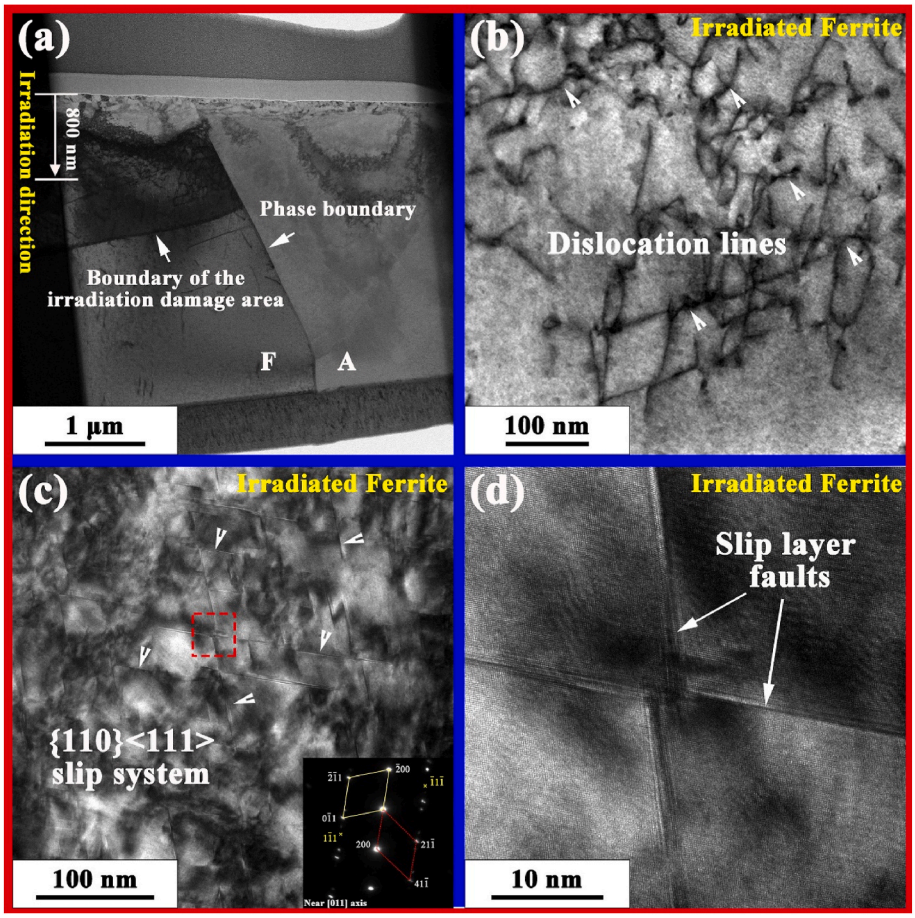

Fig. 4. TEM images of Z3CN20.09M CDSS alloys after thermal aging at 400 °C for 500 h and then irradiated by H ions at RT temperature.

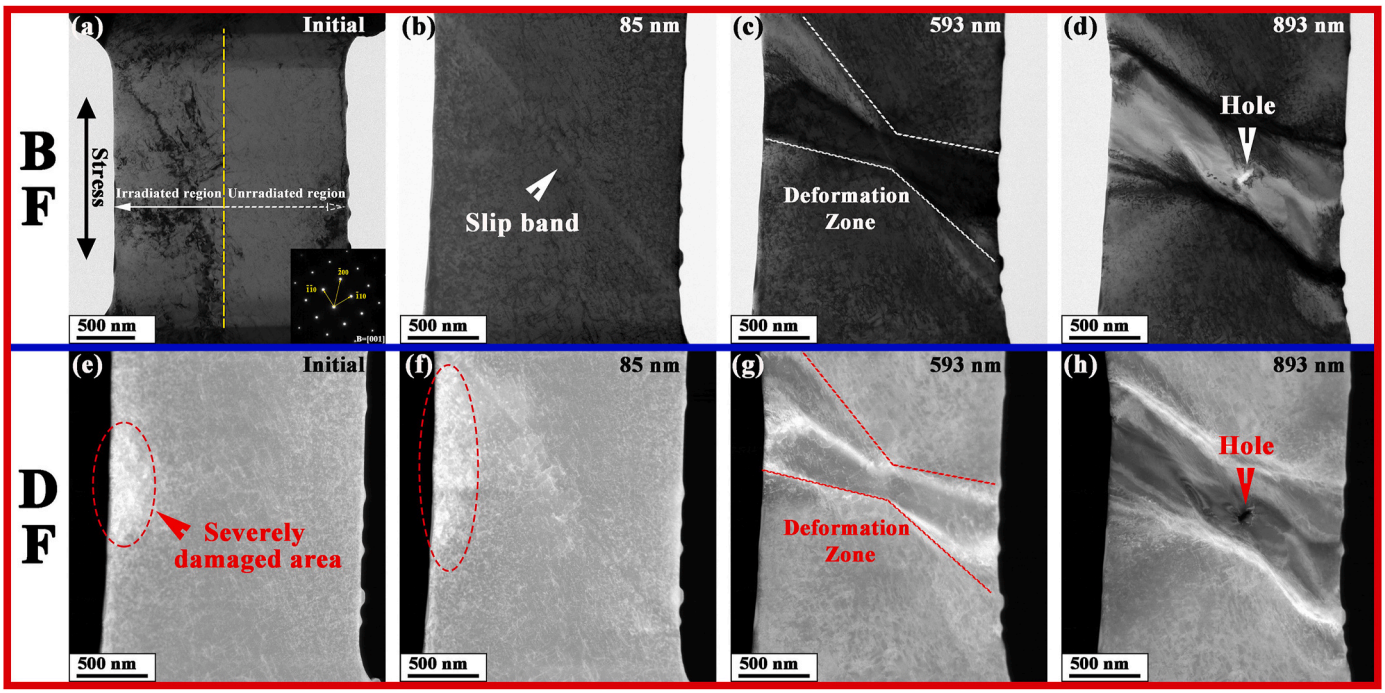

Fig. 5. Overview bright field (BF) and dark field (DF) TEM images of H ions irradiated Z3CN20.09M CDSS sample that aged at 400 °C for 500 h during the in-situ stretching process.

shown in Fig. 5(c), indicating that a large area of dislocation accumulation occurred in the vicinity of the original slip line and the narrow area in the center may have undergone torsional deformation. In addition, the dark field image Fig. 5(g) shows that the original hydrogen induced damage zone disappeared during the stretching process. When the stretching length increased up to 893 nm, a small hole formed at the deformation center area, as seen in Fig. 5(d and (h). At the same time, the dislocation accumulation region has migrated to both sides of the plastic deformation region. From the overall morphological changes, it can be seen that in the later stage of stretching, the influence of hydrogen on the sample can be almost ignore.

The magnified TEM images of the hydrogen irradiation damage zone that near the surface at the early stage of the stretching process are shown in Fig. 6. Before irradiation, very few dislocation defects were inside the unirradiated ferrite, as seen in Fig. 2(b). But after H ions irradiation, a large number of defects such as clusters and dislocations were produced in the damaged area of the irradiated sample, as seen in Fig. 6(a) and **(d).** During the entire stretching process, dislocation lines

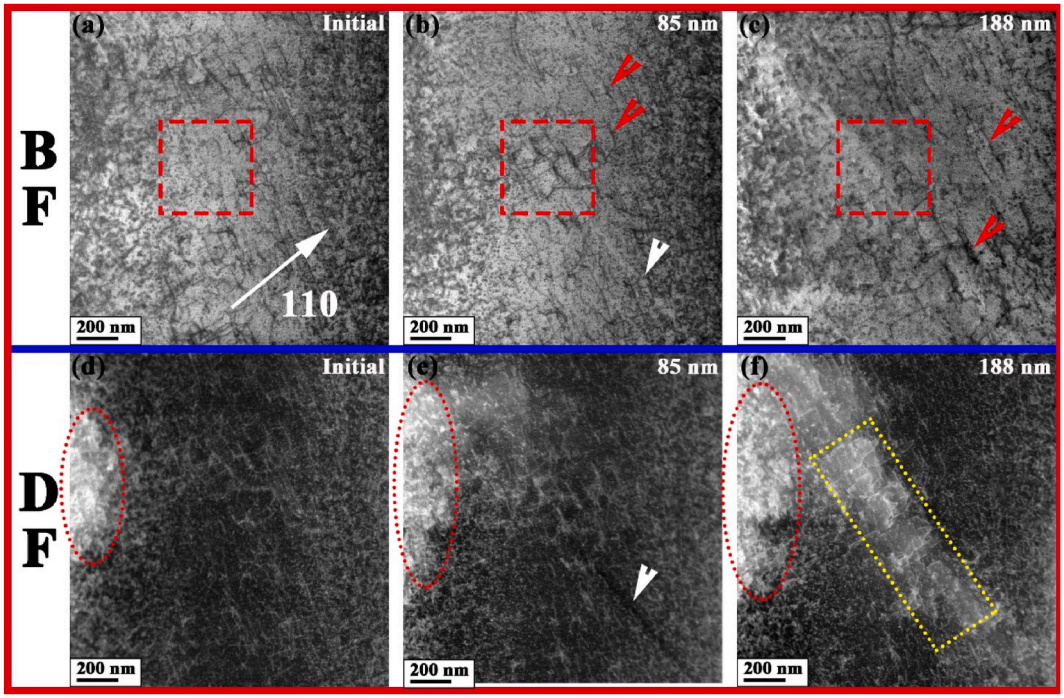

Fig. 6. Enlarged surface region TEM images of the thermal aged and H ions irradiated Z3CN20.09M CDSS alloys during the in-situ stretching process.

inside the material continuously generated, migrated, and grew up, as marked by the red boxes and red arrows in Fig. 6(a)~(c). In addition, when the elongation reached 85 nm, by comparing the positions indicated by the red arrows in the BF image Fig. 6(b) and DF image Fig. 6(d), it can be seen that a slip band perpendicular to the <110> direction gradually formed, which is consistent with the direction of the slip planes induced by hydrogen irradiation, as indicated by Fig. 4. And when the elongation increased up to 188 nm, a large number of dislocation defects accumulated at the slip band region, and significant plastic deformation has occurred, as indicated by the yellow box in Fig. 6 (f). Meanwhile, the evolutions of the near surface region enriched with the hydrogen also revealed the plastic deformation process of the stretch sample, as marked by a red ellipse in Fig. 6(d)~(f).

The magnified TEM images of the interface region that between the irradiated and unirradiated areas at the later stage of the stretching process are shown in Fig. 7. As mentioned above, when the elongation reached 593 nm, the center of the area where torsional deformation occurs is marked by a red circle, with a large number of dislocation lines parallel and perpendicular to the <110> direction clearly visible. The deformation region is shown in Fig. 7(a) and **(e)**. When the elongation increased up to 808 nm, dense dislocation lines interweaved on both sides of the deformation core area, and the region of crack initiation is marked in Fig. 7(b) and **(f)**. The sample cracked and formed a small hole when the stretching length reached 893 nm, with the crack tip pointing towards the side of the irradiated area, as seen in Fig. 7(c) and **(g)**. Fig. 7 (d) and **(h)** indicate that cracks mainly propagated along the crack tip as the stretching progressed, ultimately leading to the sample fracture. This suggests that the irradiation damage and slip system structures within the irradiation-damaged zone may accelerate crack propagation and ultimately lead to failure.

4. Conclusion

Z3CN20.09M duplex stainless steels were After thermal aging process at 400 °C and hydrogen ions irradiation, the evolutions of the microstructure and nano mechanical properties were researched and analyzed.

The nanohardness of the ferrite phase increased with the increase of thermal aging time, which is due to the segregation of the Fe and Cr elements induced by spinodal decomposition. The nanohardness of the damaged region in the irradiated Z3CN20.09M samples further increased after the injection of hydrogen ions. However, the hydrogen ion implantation weakened the hardening effect induced by the spinodal decomposition during thermal aging process. This reduction in hardening is due to the formation of a large number of {011}<111> slip system structures, which significantly suppress the hardening effects caused by ion irradiation-induced dislocations and element segregation from spinodal decomposition.

During the in-situ tensile test of TEM, with the increase of the stretching length, a slip band that runs diagonally through the entire sample region firstly appeared, and then a large area of dislocation accumulated in the vicinity of the slip band. As the stretching experiment progressed, severe deformation occurred and extended along this slip band. When the stretching length increased up to 893 nm, a cracking formed at the deformation center area, and further propagated along the crack tip towards the irradiation damage side, ultimately leading to the sample fracture.

In general, the results in this work indicate that hydrogen ion implantation can further deteriorate the mechanical properties of materials, but to some extent, it can weaken the hardening effect of materials induced by the spinodal decomposition during the thermal aging process. And cracking tends to occur at the interface region between the irradiated and non irradiated areas and propagate towards the irradiated damage side.

CRediT authorship contribution statement

Penghui Lei: Writing – original draft, Software, Methodology. **Ni Jiang:** Data curation, Conceptualization. **Jiannan Hao:** Visualization. **Qing Peng:** Writing – review & editing, Investigation. **Pan Qi:** Project administration, Investigation. **Fangjie Shi:** Resources. **Yuhua Hang:** Methodology. **Qianwu Li:** Conceptualization. **Chao Ye:** Writing – review & editing, Investigation.

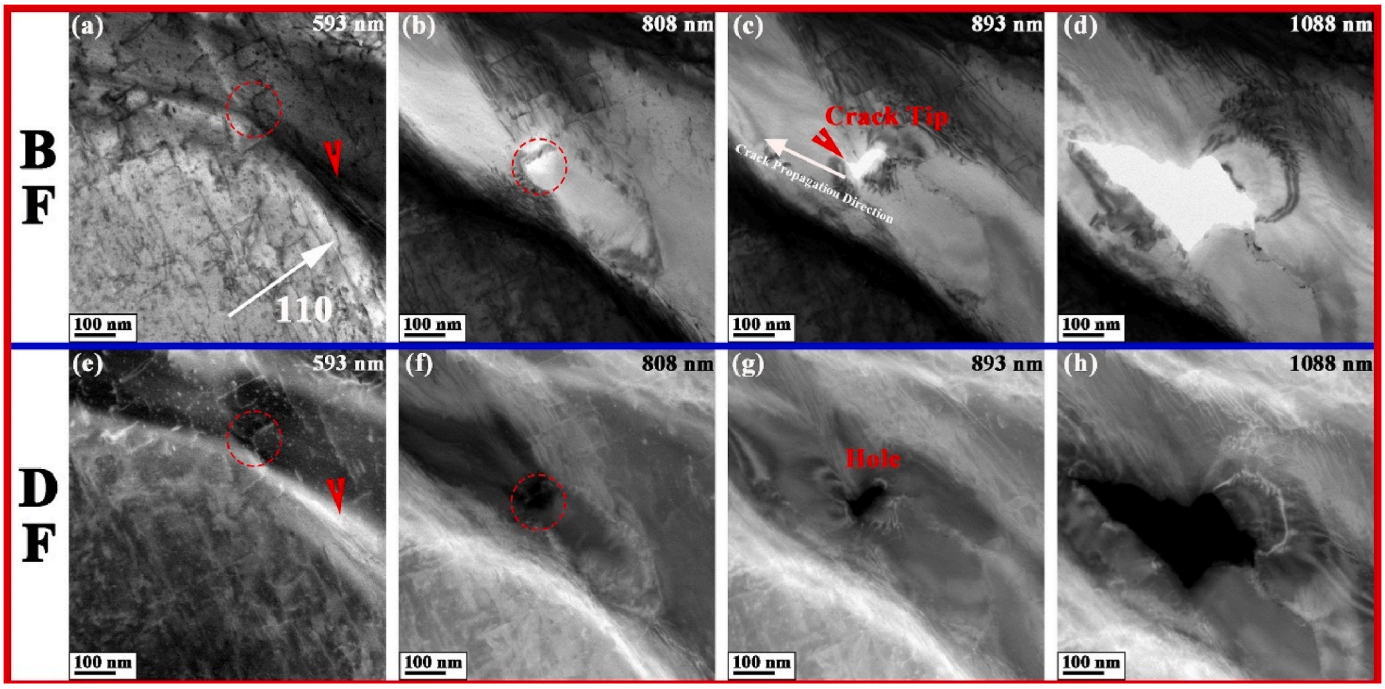

Fig. 7. Enlarged TEM images of the interface region between the irradiated and unirradiated areas in the thermal aged and H ions irradiated Z3CN20.09M CDSS alloys during the in-situ stretching process.

Declaration of competing interest

We declare that we have no known competing financial interests or personal relationships that could have appeared to influence the work reported in this paper entitled “Effect of hydrogen ion irradiation on the mechanical properties of the thermal aged Z3CN20.09M duplex stainless steel”.

Acknowledgements

This work is supported by the National Key Research and Development Program of China (Grant No. 2022YFB3707200), the National Natural Science Foundation of China (No. 12205236), the Strategic Priority Research Program of Chinese Academy of Sciences (Grant No. XDB0620103), National Natural Science Foundation of China (Grant No. 12272378), and High-level Innovation Research Institute Program of Guangdong Province (Grant No. 2020B0909010003).

Data availability

The data that has been used is confidential.

References

[1] Y. Yao, J. Wei, Z. Wang, Effect of long-term thermal aging on the mechanical properties of casting duplex stainless steels, Mater. Sci. Eng. 551 (2012) 116–121.
[2] X. Chen, D. Tian, L. Ling, T. Liu, H. Wang, Y. Chen, Y. Lu, Microstructure and corrosion resistance of Z3CN20. 09M stainless steels after different thermo-mechanical processing, J. Nucl. Mater. 577 (2023) 154300.
[3] Y. Wang, Y. Yao, Z. Wang, Y. Jin, X. Zhang, J. Liu, Thermal ageing on the deformation and fracture mechanisms of a duplex stainless steel by quasi in-situ tensile test under OM and SEM, Mater. Sci. Eng. 666 (2016) 184–190.
[4] Y. Fan, T. Liu, L. Xin, Y. Han, Y. Lu, T. Shoji, Thermal aging behaviors of duplex stainless steels used in nuclear power plant: a review, J. Nucl. Mater. 544 (2021) 152693.
[5] S. Chen, Y. Miyahara, A. Nomoto, K. Nishida, Effects of thermal aging and low-fluence neutron irradiation on the mechanical property and microstructure of ferrite in cast austenitic stainless steels, Acta Mater. 179 (2019) 61–69.
[6] J.D. Tucker, M.K. Miller, G.A. Young, Assessment of thermal embrittlement in duplex stainless steels 2003 and 2205 for nuclear power applications, Acta Mater. 87 (2015) 15–24.
[7] J. Shiao, C. Tsai, J. Kai, J. Huang, Aging embrittlement and lattice image analysis in a Fe-Cr-Ni duplex stainless steel aged at 400 C, J. Nucl. Mater. 217 (3) (1994) 269–278.
[8] S. Li, Y. Wang, X. Wang, Effects of ferrite content on the mechanical properties of thermal aged duplex stainless steels, Mater. Sci. Eng. 625 (2015) 186–193.
[9] T.S. Byun, D.A. Collins, T.G. Lach, E.L. Carter, Degradation of impact toughness in cast stainless steels during long-term thermal aging, J. Nucl. Mater. 542 (2020) 152524.
[10] M. Li, S. Zhong, X. Shang, H. Zhai, L. Li, S. Wang, Hydrogen diffusion and precipitation influenced by non-uniformly distributed stress in zirconium alloy with different textures, J. Nucl. Mater. (2024) 155204.
[11] S. Uchida, M. Naitoh, H. Okada, Y. Hanamoto, Effects of oxide layers on zirconium alloy-steam reaction, Journal of Radiation Research and Applied Sciences 16 (3) (2023) 100617.
[12] Z. Cao, G. Ran, Z. Wang, Y. Li, X. Wu, L. Wu, X. Huang, H. Mo, In-situ TEM study on the evolution of dislocation loops and bubbles in CeO2 during Kr+ single-beam and Kr+-H2+ dual-beam synergetic irradiation, J. Mater. Sci. Technol. 123 (2022) 49–59.
[13] I. Ali, G. Imanova, T. Agayev, A. Aliyev, T.A. Kurniawan, M.A. Habila, Radiation-catalytic activity of zirconium surface during water splitting for hydrogen production, Radiat. Phys. Chem. 224 (2024) 112002.
[14] M.-H. Yun, J.-W. Yeon, Electrochemical behavior of dissolved hydrogen at Pt electrode surface in a high temperature LiOH–H3BO3 solution: effect of chloride ion on the transient current of the dissolved hydrogen, Nucl. Eng. Technol. 55 (10) (2023) 3659–3664.
[15] G. Jiang, D. Xu, W. Yang, L. Liu, S. Guo, S. Wang, Incipient corrosion of FeCrAl alloys in H3BO3-and LiOH-containing pure water at 360° C and 18.5 MPa, J. Nucl. Mater. 557 (2021) 153299.
[16] Y. Sanada, K. Oshikiri, M. Kanno, T. Abe, Development of a practical tritiated water monitor to supervise the discharge of treated water from Fukushima Daiichi Nuclear Power Plant, Nucl. Instrum. Methods Phys. Res. Sect. A Accel. Spectrom. Detect. Assoc. Equip. 1062 (2024) 169208.
[17] S. Jing, S. Xueyao, L. Shengsheng, W. Hui, Research on hydrogen risk prediction in probability safety analysis for severe accidents of nuclear power plants, Nucl. Eng. Des. 417 (2024) 112798.
[18] J. Liang, Q. Wei, F. Ge, D. Ren, J. Wang, Y. Dong, P. Eklund, F. Huang, S. Du, Q. Huang, Synthesis of Zr2Al3C4 coatings on zirconium-alloy substrates with AlC/Si interlayers as diffusion barriers, Vacuum 160 (2019) 128–132.
[19] Y. Deng, H. Liao, Y. He, Y. Yin, M. Pellegrini, G. Su, K. Okamoto, Y. Wu, Investigation on hydrogen embrittlement and failure characteristics of Zr-4 cladding based on the GTN method, Nuclear Materials and Energy 36 (2023) 101463.
[20] S. Kim, J.-H. Kang, Y. Lee, Hydride embrittlement resistance of Zircaloy-4 and Zr-Nb alloy cladding tubes and its implications on spent fuel management, J. Nucl. Mater. 559 (2022) 153393.
[21] H. Sun, Y. Zhang, X. Zhu, C. Xu, C. Sun, B. Luan, Study of oxidation behavior and associated microstructure evolution of Zircaloy-4 exposed to high temperature pure steam, Vacuum 211 (2023) 111892.
[22] Z. Que, H. Seifert, V. Mazánová, P. Spätig, Hydrogen embrittlement on fracture resistance of low-alloy reactor pressure vessel steel with high dynamic strain aging at 288° C, Mater. Lett. 308 (2022) 131269.
[23] G. Rao, Y. Yagodzinskyy, Z. Que, P. Spätig, H. Seifert, Study on hydrogen embrittlement and dynamic strain ageing on low-alloy reactor pressure vessel steels, J. Nucl. Mater. 556 (2021) 153161.
[24] Y. Zhao, Y. Lu, X. Zhang, Z. Li, T. Liu, T. Shoji, Effects of dissolved hydrogen on corrosion fatigue crack growth behavior of 316LN stainless steel in high temperature pressurized water environment, Corrosion Sci. 232 (2024) 112041.
[25] D. Kim, D. Woo, Y. Lee, Radial hydride fraction with various rod internal pressures and hydrogen contents for Zr-Nb alloy cladding tube, J. Nucl. Mater. 572 (2022) 154036.
[26] K.R. Nantes, M. Jin, A.T. Motta, Modeling hydrogen localization in Zircaloy cladding subjected to temperature gradients, J. Nucl. Mater. 589 (2024) 154853.
[27] B.M. Şeşen, M. Mansoor, C. Örnek, Elucidating the dynamics of hydrogen embrittlement in duplex stainless steel, Corrosion Sci. 225 (2023) 111549.
[28] T. Pogrielz, M. Eichinger, A. Weiser, J. Todt, A. Hohenwarter, A. Ascii, B. Sarac, D. Brandl, G. Ressel, M. Jary, Peculiarity of hydrogen absorption in duplex steels: phase-selective lattice swelling and stress evolution, Scripta Mater. 248 (2024) 116142.
[29] X. Yan, Z. Li, P. Lei, S. Wang, R. Gao, Significant suppression of helium bubbles in oxide dispersion strengthened FeCrAl alloys irradiated by high concentration of helium, Vacuum 221 (2024) 112915.
[30] E. Lu, X. Cao, S. Jin, C. Zhang, P. Zhang, L. Guo, T. Zhu, Y. Gong, B. Wang, The evolution of micro defects in He+ irradiated FeCrNi alloy during isochronal annealing, Nucl. Instrum. Methods Phys. Res. Sect. B Beam Interact. Mater. Atoms 356 (2015) 94–98.
[31] J. Zhou, J. Odqvist, M. Thuvander, S. Hertzman, P. Hedström, Concurrent phase separation and clustering in the ferrite phase during low temperature stress aging of duplex stainless steel weldments, Acta Mater. 60 (16) (2012) 5818–5827.
[32] C. Lu, Z. Yang, F. Chen, M. Fan, P. Huang, G. Ge, X. Tang, Phase-field simulation of the microstructure and properties evolution in cast austenitic stainless steels for nuclear power plants during thermal aging and annealing, Nucl. Eng. Des. 415 (2023) 112604.
[33] J. Shi, F. Xue, Q. Peng, Y. Shen, A phase-field study on spinodal decomposition of ferrite of Fe-Cr-Ni stainless steels during thermal ageing and annealing, Chin. J. Mater. Res. 34 (5) (2020) 328–336.
[34] A. Takahashi, T. Suzuki, A. Nomoto, T. Kumagai, Influence of spinodal decomposition structures on the strength of Fe-Cr alloys: a dislocation dynamics study, Acta Mater. 146 (2018) 160–170.
[35] Q. Chang, Q. Peng, J. Hao, P. Qi, P. Lei, N. Jiang, C. Ye, Damage microstructures in Ti3SiC2 under successive Xe-He-H ions irradiation and annealing process, J. Nucl. Mater. (2024) 155235.
[36] Y. Zhang, G.M. Stocks, K. Jin, C. Lu, H. Bei, B.C. Sales, L. Wang, L.K. Béland, R. E. Stoller, G.D. Samolyuk, Influence of chemical disorder on energy dissipation and defect evolution in concentrated solid solution alloys, Nat. Commun. 6 (1) (2015) 8736.
[37] K. Tomatsu, T. Omura, Y. Nishiyama, Y. Todaka, Influence of hydrogen on local mechanical properties of pure Fe with different dislocation densities investigated by electrochemical nanoindentation, ISIJ Int. 56 (12) (2016) 2298–2303.
[38] Y. Zhao, M.-Y. Seok, I.-C. Choi, Y.-H. Lee, S.-J. Park, U. Ramamurty, J.-Y. Suh, J.-i. Jang, The role of hydrogen in hardening/softening steel: influence of the charging process, Scripta Mater. 107 (2015) 46–49.
[39] K. Tomatsu, T. Amino, T. Chida, S. Uji, M. Okonogi, H. Kawata, T. Omura, N. Maruyama, Y. Nishiyama, Anisotropy in hydrogen embrittlement resistance of drawn pearlitic steel investigated by in-situ microbending test during cathodic hydrogen charging, ISIJ Int. 58 (2) (2018) 340–348.
[40] K. Miyata, Effect of hydrogen charging on dislocation behavior in Ni-Cr and Ni 2 Cr alloys, Metall. Mater. Trans. 34 (2003) 1249–1257.
[41] H.K. Birnbaum, P. Sofronis, Hydrogen-enhanced localized plasticity—a mechanism for hydrogen-related fracture, Mater. Sci. Eng. 176 (1–2) (1994) 191–202.
[42] P. Sofronis, H.K. Birnbaum, Mechanics of the hydrogendashdislocationdashimpurity interactions—I. Increasing shear modulus, J. Mech. Phys. Solid. 43 (1) (1995) 49–90.
[43] A. Barnoush, H. Vehoff, In situ electrochemical nanoindentation: a technique for local examination of hydrogen embrittlement, Corrosion Sci. 50 (1) (2008) 259–267.
[44] A. Barnoush, H. Vehoff, Recent developments in the study of hydrogen embrittlement: hydrogen effect on dislocation nucleation, Acta Mater. 58 (16) (2010) 5274–5285.